Journal of Materials Chemistry A

Accepted Manuscript

ROYAL SOCIETY OF CHEMISTRY

www.rsc.org/materialsA

Journal Name

RSCPublishing

ARTICLE

Magnetic Yolk-Shell Mesoporous Silica Microspheres with Supported Au Nanoparticles as Recyclable High-Performance Nanocatalysts

Cite this: DOI: 10.1039/x0xx00000x

Received 00th January 2012,
Accepted 00th January 2012

DOI: 10.1039/x0xx00000x

www.rsc.org/

Q. Yue,[a] Y. Zhang,[a] C. Wang,[a] X. Q. Wang,[a] Z. K. Sun,[a] X. F. Hou,[a] D. Y. Zhao,[a] and Y. H. Deng[*a]

Based on the surface engineering strategy, multifunctional yolk-shell microspheres with a magnetic core encapsulated in a hollow mesoporous silica have been rationally synthesized through a stepwise solution-phase interface deposition approach by combining the sol-gel chemistry and surfactant-involved co-assembly process. The resulting microspheres possess well-defined yolk-shell structure, uniform sizes, high magnetization (~ 23.5 emu/g), perpendicularly aligned mesopore channels (~ 2.2 nm in diameter), high surface area (~ 405 m2/g) and controllable void space size (320 ~ 430 nm in diameter). Gold nanoparticles of 4.2 nm are incorporated into the yolk-shell microspheres, leading to a novel magnetically recyclable nanocatalyst. The obtained catalyst exhibits an excellent catalytic performance for styrene epoxidation with high conversion (91.4 %) and selectivity (83.1 %) in 12 h, much better than its counterpart Au-loaded magnetic mesoporous silica catalyst. The multifunctional yolk-shell microspheres possess a superior stability in terms of catalysis performance and porous yolk-shell structure even after 12 cycles of catalysis.

Introduction

The designed fabrication of nanostructured materials by integrating different functional building blocks on nanoscale is highly important to develop high-performance catalysts, energy storage systems, and diagnosis and therapy nanotools[1-3]. Ordered mesoporous materials synthesized based on the supra-molecule-templating approach have attracted considerable research interest due to their outstanding features (high surface, large pore volume and uniform pore sizes) and potential applications in various fields, especially for supporting nanocatalysts [4-8]. Gold nanoparticles have shown exceptional catalytic activities for many reactions, owing to their high surface-to-volume ratio and a large fraction of metal atoms that are exposed to reactant molecules.[9-18] However, gold nanoparticles have a large tendency to aggregate driven by van der Waals forces and high interface energy because of their ultrasmall particle size.[18, 19] Additionally, as an intriguing nanocatalyst in liquid reaction solutions, the valuable gold nanoparticles are easy to be flushed away during the recycling process, leading to the waste of catalysts and the contamination of products. Thus, a great variety of strategies have been exploited to immobilize Au nanoparticles in or onto solid supports. Direct deposition of Au nanoparticles on supports like alumina and titania helps to form highly dispersed catalytic centers, but the migration and sintering of Au species at high temperature is inevitable.[20, 21] Although loading into the pore channels of mesoporous materials can effectively prevent aggregation of Au nanoparticles during reactions, it could impede the diffusion of reactants and products.[22] Coating Au nanoparticles with a shell of mesoporous silica to construct core-shell structure is also an effective method to prevent the agglomeration of gold nanoparticles;[23-25] however, the nanoparticle's surface is not fully available for catalysis because their surfaces are partly covered by silica. Therefore, it is highly desired to design advanced Au-based composite nanocatalysts with stably immobilized, well-dispersed, and accessible Au nanoparticles, so as to fully implement their catalytic functions

Taking the above considerations into account, composite nanocatalysts with yolk-shell structure have been recently recognized as an ideal candidate for catalysis applications.[26-34] Particularly, yolk-shell microspheres with a movable functional core and mesoporous shell possess unique advantages and structure configuration, because they have a solid core for immobilizing gold nanoparticle or anchoring guest biomacromolecules (e. g. enzymes), tunable hollow spaces for accommodation of guest molecules, and mesoporous shell for preventing the confined nano-objects (gold nanoparticles, enzymes) from being leached. To date, although there are reports about the synthesis of yolk-shell structured microspheres for controlled delivery system,[35-40] catalysis,[41-47] biotherapy,[48,49] and lithium battery,[50-54] it still remains a grand change to synthesize yolk-shell microspheres with well-defined and controllable structure, and little work has been done to

effectively immobilize nanocatalyst on the functional yolk and investigate the confinement effect on catalysis.

Herein, for the first time, we report the designed synthesis of a novel kind of yolk-shell microspheres consisting of silica-coated magnetite (Fe_3O_4@SiO_2) materials supported Au nanoparticles and mesoporous silica. This yolk-shell mesoporous support was constructed through a controllable stepwise interface deposition and surfactant-templating co-assembly process. The obtained multifunctional microspheres, denoted as Fe_3O_4@SiO_2@hollow $mSiO_2$ microspheres, possess a movable silica-protected magnetic core (~ 270 nm), tunable hollow spaces (320-430 nm in diameter), highly accessible mesopore channels (~ 2.2 nm), high surface area (405-435 m^2/g) and large magnetization (19.3-23.5 emu/g). Through an in-situ deposition of sub-5 nm Au nanoparticles on the Fe_3O_4@SiO_2 yolk, novel nano-catalysts with highly integrated functionalities were obtained, which exhibit excellent catalytic performances in styrene epoxidation with high conversion of styrene (91.4 %) and good selectivity to styrene oxide (83.1 %) in 12 h. Through a simple magnetic separation, the yolk-shell nanocatalysts can be easily recycled with a magnetic field, and reused for catalysis without significant reduction of the catalytic performance even after use for 12 times.

Experimentals

Chemicals

Anhydrous $FeCl_3$, trisodium citrate, sodium acetate, tetraethyl orthosilicate (TEOS), Resorcinol, formaldehyde, $HAuCl_4$•$3H_2O$, ethanol, ethylene glycol, concentrated ammonia solution (28 wt %) are of analytical grade (Shanghai Chemical Corp.). Cetyltrimethyl ammonium bromide (CTAB) and *tert*-Butyl hydroperoxide (70 wt % in water) was supplied by Aldrich-sigma. Styrene was purified by filtrating through Al_2O_3 column. All other chemicals were used as received. Deionized water was used for all experiments.

Synthesis of yolk-shell Fe_3O_4@SiO_2@hollow $mSiO_2$ microspheres

Synthesis of Fe_3O_4 particles. The hydrophilic Fe_3O_4 particles were synthesized according to the method reported previously.[55] Briefly, $FeCl_3$•$6H_2O$ (3.25 g), trisodium citrate (1.3 g), and sodium acetate (NaAc, 6.0 g) were dissolved in ethylene glycol (100 mL) with magnetic stirring. The obtained yellow solution was then transferred and sealed into a Teflon-lined stainless-steel autoclave (200 mL in capacity). The autoclave was heated at 200 °C for 10 h, and then allowed to cool down to room temperature. The black products were washed with deionized water and ethanol 3 times, respectively.

Synthesis of Fe_3O_4@SiO_2 microsphere. An aqueous dispersion of the magnetite particles (70 mL, 0.02 g/mL) was added to a three-neck round-bottom flask charged with absolute ethanol (280 mL) and concentrated ammonia solution (5.0 mL, 28 wt %) under mechanical stirring for 15 min at 30 °C. Afterward, 4.0 mL of TEOS) was added dropwise in 2 min, and the reaction was allowed to proceed for 8 h under continuous mechanical stirring. The mole ratio of TEOS: NH_4OH: EtOH: H_2O is 1.9: 4.0: 487: 389. The resultant core-shell Fe_3O_4@SiO_2 microsphere product was separated and collected with a magnet, followed by washing with ethanol 6 times.

Synthesis of Fe_3O_4@SiO_2@RF microspheres. 100 mg of Fe_3O_4@SiO_2 microspheres was dispersed in a mixture solution of ethanol (20 mL) and deionized water (10 mL) by ultrasonication. Into the resulting dispersion, ammonium hydroxide aqueous solution (0.5 g, 28 wt %), resorcinol (0.1 g, 0.09 mM), and formaldehyde (0.1 g, 37 wt %) were added consecutively, and the mixed dispersion was mechanically stirred for polymerization for 2 h at 30 °C, forming a layer of resorcinol formaldehyde (RF) resin on the seed. The mole ratio of resorcinol: formaldehyde: NH_4OH: EtOH: H_2O is 0.9: 1.2: 4: 350: 556. After polymerization, the obtained Fe_3O_4@SiO_2@RF microspheres were collected by a magnet and washed with deionized water/alcohol three times, respectively. To tune the RF shell thickness, the concentration of the RF precursor (with a ratio of resorcinol to formaldehyde at 1:1) was increased from 6 mg/mL to 20 mg/mL.

Synthesis of Fe_3O_4@SiO_2@hollow $mSiO_2$ microspheres. In a typical synthesis, the as-made Fe_3O_4@SiO_2@RF microspheres (0.12 mg) were redispersed in a mixed solution containing CTAB (0.45 g, 1.2 mmol), deionized water (100 mL), concentrated ammonia solution (2.0 mL, 28 wt %), and ethanol (150 mL). The resultant mixed solution was ultrasonicated for 5 min and then mechanically stirred for 30 min to form a homogeneous dispersion. Subsequently, 1.5 mL of TEOS was added dropwise to the dispersion under continuous stirring. The mole ratio of CTAB: TEOS: NH_4OH: EtOH: H_2O is 1.2: 7.2: 16: 2600: 5500. After stirring for 6 h at 30 °C, the product was collected with a magnet and washed repeatedly with ethanol and deionized water. The obtained sample was dried in vacuum at 40 °C for 12 h and calcined at 550 °C in air for 5 h to remove CTAB and RF, and yolk-shell magnetic mesoporous silica, i. e. Fe_3O_4@SiO_2@hollow $mSiO_2$ microspheres, were finally obtained.

Loading Au nanoparticles into the Fe_3O_4@SiO_2@hollow $mSiO_2$ microspheres for catalysis

Au nanoparticles were loaded into the yolk-shell magnetic mesoporous silica microspheres via an in situ reduction method.[56] Typically, 50 mg of ethylenediamine (en) was added to the aqueous solution of $HAuCl_4$•$4H_2O$ (0.10 g in 1.0 g of H_2O) to form a transparent brown solution. After stirring for 30 min, 8 mL of ethanol was added to precipitate the $AuCl_3(en)_2$ compound. The product was filtered, washed with ethanol and dried in vacuum at 40 °C. A solution was prepared by dissolving 10 mg of $AuCl_3(en)_2$ in 5 mL of H_2O, and the pH value of the solution was adjusted to 10.0 by adding NaOH solution (5.0 wt %). Subsequently, 100 mg of Fe_3O_4@SiO_2@hollow $mSiO_2$ microspheres with hollow space size of ~ 320 nm (denoted as YS-320) was added. After stirring for 1 h, the sample was separated by centrifugation, dried in a vacuum oven at 40 °C for 48 h, and finally reduced by flowing H_2/Ar (5.0 %) at 150 °C for 1 h, resulting in Au nanoparticles loaded microspheres, denoted as YS-320-Au (see ref. 56 for

detailed reaction mechanism). Following the same synthesis procedure, YS-370-Au and YS-430-Au catalysts with the same Au loading were synthesized.

Catalytic epoxidation of styrene

10 g of catalyst was added to a mixture of styrene (2.6 mL, 20 mmol), and acetonitrile (10 mL). The dispersion was bubbled with high purity N_2 for 30 min at room temperature. After adding 10.0 g (76 mmol) of *t*-butyl hydroperoxide (70 wt % in water), the reaction vessel was immersed in an oil bath and heated at 82 °C. During the reaction process, a minor amount of reaction solution (20 μL) was withdrawn at different time intervals for gas chromatography-mass spectrometer (GC-MS) measurements. After reaction for 40 h, the reaction system was cooled down, and the catalyst was recycled using a magnet, and washed with acetonitrile 3 times, vacuum dried at 40°C for reuse.

Measurements and characterization

Transmission electron microscopy (TEM) experiments were conducted on a JEOL 2011 microscope (Japan) operated at 200 kV. Scanning electron microscopy (SEM) images were collected with Philips XL30 electron microscope operated at 20 kV. A thin gold film was sputtered on the samples before SEM measurements. Powder X-ray diffraction (XRD) patterns were recorded on a Bruker D4 X-ray diffractometer (Germany) with Ni-filtered Cu KR radiation (40 kV, 40 mA). Nitrogen sorption isotherms were measured at 77 K with a Micromeritcs Tristar 3000 analyzer. Before measurements, the samples were degassed in a vacuum at 200 °C for 10 h. The Brunauer-Emmett-Teller (BET) method was utilized to calculate the specific surface areas (SBET) using adsorption data in a relative pressure range from 0.005 to 0.25. By using the Barrett-Joyner-Halenda (BJH) model, the pore volumes and pore size distributions were derived from the adsorption branches of isotherms, and the total pore volumes (Vt) were estimated from the adsorbed amount at a relative pressure P/P_0 of 0.992. The metal contents in the Fe_3O_4@SiO_2@hollow $mSiO_2$–Au samples were measured using inductively coupled plasma-atomic emission spectrometry (ICP-AES, Varian VISTA-MPX).

Results and Discussion

The overall synthesis procedure for the multifunctional yolk-shell microspheres involves four steps as depicted in Scheme 1. Firstly, water dispersible magnetite particles were coated by a protecting layer of the condensed silica, forming core-shell Fe_3O_4@SiO_2 microspheres. Secondly, a layer of resorcinol-formaldehyde (RF) resin was deposited on the surface of Fe_3O_4@SiO_2 microspheres through interface polymerization of resorcinol and formaldehyde catalyzed by ammonium hydroxide due to electrostatic attraction between resorcinol derivatives and NH_4^+ ions absorbed on Fe_3O_4@SiO_2 microspheres.[57] Thirdly, the resultant Fe_3O_4@SiO_2@RF microspheres were further coated by a layer of CTAB/silica composite via a surfactant-templated sol-gel coating process using CTAB as the template and TEOS as the silica precursor. Fourthly, RF resin and CTAB were removed through calcination in air at 550 °C, and the yolk-shell Fe_3O_4@SiO_2@hollow $mSiO_2$ microspheres were obtained. Finally, Au nanoparticles were immobilized onto the Fe_3O_4@SiO_2 yolk through adsorption of gold precursor on the yolk and subsequent reduction treatment in hydrogen.

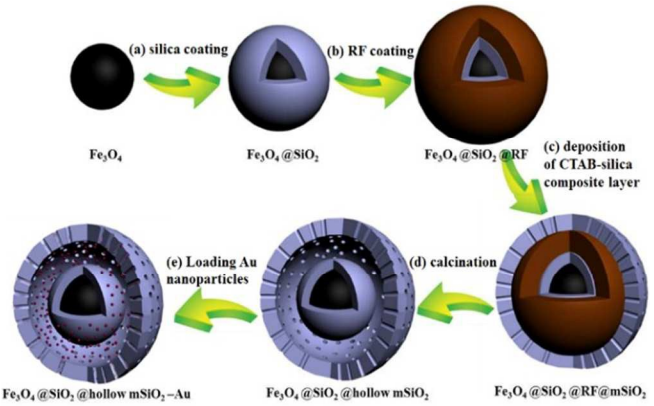

Scheme 1 The synthetic procedure for the multifunctional yolk-shell magnetic mesoporous silica microspheres with gold nanoparticles embedded in the voids. (a) coating magnetite particles with silica through a sol-gel process of TEOS, (b) deposition of RF polymer layer on the core-shell Fe_3O_4@SiO_2 microspheres, (c) further deposition of CTAB-SiO_2 composite layer via the surfactant-templated sol-gel process, (d) removal of CTAB and RF resin through calcination treatment, forming yolk-shell mesoporous silica microspheres, (e) loading Au nanoparticles *via* an in-situ reduction method.

The hydrophilic magnetite particles were synthesized through a well-established solvothermal reaction based on a high temperature reduction of $FeCl_3$ with ethylene glycol in the presence of trisodium citrate as a stabilizer at 200 °C.[56] The obtained magnetite particles have a mean diameter of ~ 150 nm (Figure 1a). Due to the chelating effect of citrate groups, the obtained magnetite particles stabilized by citrate groups possess excellent water dispersibility, which is favorable for surface modification via a solution-phase synthesis. Through the well-known Stöber coating approach, a uniform silica shell was deposited on the magnetite particles via the hydrolysis and condensation of TEOS in a basic ethanol-water mixture. The resultant Fe_3O_4@SiO_2 microspheres exhibit uniform core-shell structure with silica shell of ~ 60 nm in thickness, as shown in the TEM image (Figure 1b). The SEM observation (Figure 1c) reveals that the as-synthesized Fe_3O_4@SiO_2 microspheres possess regular spherical morphology with a mean diameter of about 270 nm, in good agreement with the TEM results. The coefficient of variance of particle size distribution (C_v)[58] of Fe_3O_4@SiO_2 microspheres is calculated to be 3.52% (less than 5%) based on the large-area SEM image (Figure 1c), indicating the uniform microspheres. The silica coating helps to improve the dispersibility of the magnetic particles because silica shells derived from Stöber method are highly negatively charged,[59] generating electrostatic repulsion between microspheres; meanwhile, they can serve as an insulation layer that protects the magnetite core from etching and oxidation in practical applications. After further deposition of RF resin via the polymerization of resorcinol (3.0 mg/mL) and formaldehyde (3.0 mg/mL) in the basic ethanol-water solution, a uniform RF layer with thickness of about 25 nm was uniformly generated on the core-shell Fe_3O_4@SiO_2 microspheres, forming Fe_3O_4@SiO_2@RF microspheres with a well-defined sandwich structure (Figure 1d). Interestingly, the obtained Fe_3O_4@SiO_2@RF microspheres pack into ordered structure on the silicon substrate during the preparation sample for SEM observation (Figure 1g), which is mainly due to their size

homogeneity and good dispersibility. Moreover, because of the presence of phenol hydroxyl groups in the RF surface, the core-shell Fe_3O_4@SiO_2@RF microspheres exhibit good dispersibility in polar solvents like ethanol and water (Figure 1h).

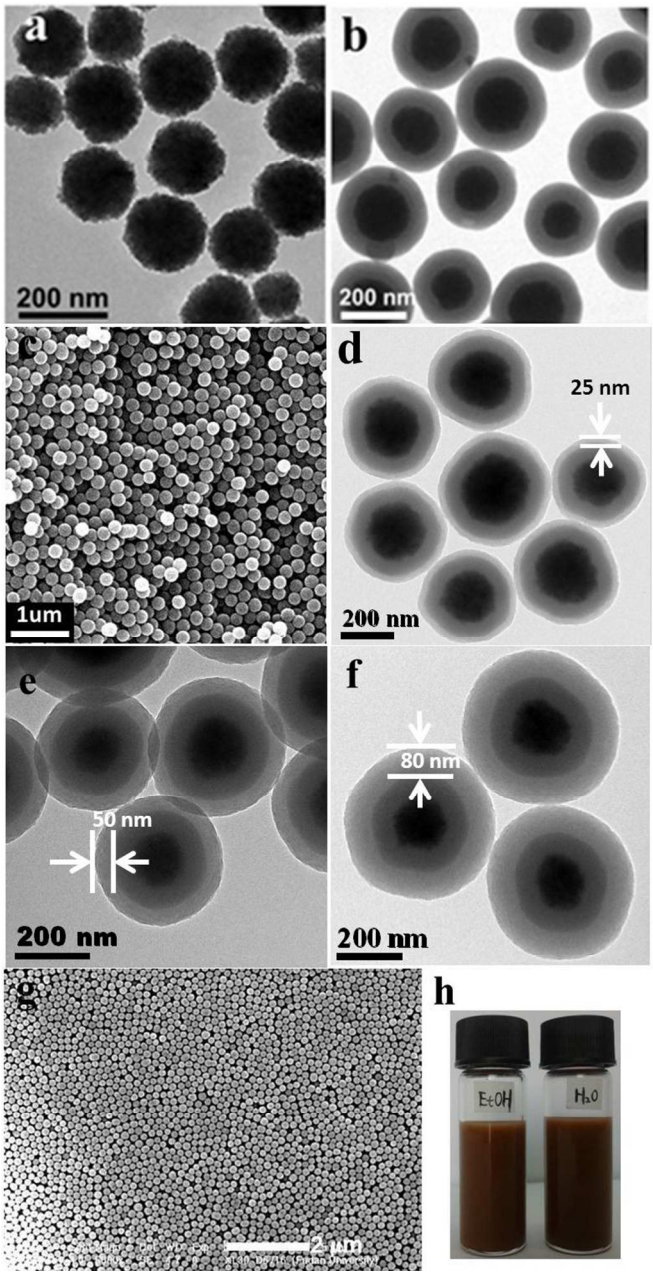

Figure 1. TEM images of the as-made F_3O_4 particles (a), the core-shell Fe_3O_4@SiO_2 microspheres (b), Fe_3O_4@SiO_2@RF microspheres with RF shell in thickness of 25, 50, 80 nm, respectively (d, e, f), SEM images of Fe_3O_4@SiO_2 microspheres (c) and the double-shelled Fe_3O_4@SiO_2@RF microspheres with 25 nm thick RF shell (g), and the optical photo of the double-shelled Fe_3O_4@SiO_2@RF microspheres dispersed in ethanol and water (h).

It is noteworthy that, by increasing the concentration of RF precursor in the reaction solution, the RF shell thickness can be easily tuned from 25 to 80 nm, and the microspheres show distinct spherical morphology regardless of the RF thickness (Figure 1e, f). Such a well-controllable growth of RF on Fe_3O_4@SiO_2 microspheres is due to the hydrogen bonding between RF precursors and silanol groups in microspheres' surface, and this makes the deposition of RF occur preferentially on the silica surface. By using Fe_3O_4@SiO_2@RF microspheres with RF thickness of ~ 25 nm as seeds, a layer of mesostructured CTAB-silica composites can be further deposited on the microspheres through the surfactant-templated sol-gel coating process involving the co-assembly of cationic surfactant CTAB and silica oligomers. The obtained multi-shelled core-shell microspheres possess an outer CTAB-silica composite shell of ~ 50 nm in thickness (Figure 2a, b). During the subsequent calcination in air, both CTAB and RF can be removed, as confirmed by Fourier transfer infrared (FTIR) spectra (Figure S1). TEM observation reveals that the obtained yolk-shell microspheres have a solid magnetic silica core-shell microsphere of ~ 270 nm, a spherical hollow space of ~ 320 nm in diameter and a mesoporous silica shell of ~ 50 nm in thickness (Figure 2c, d). High-resolution TEM image shows clearly that the ordered mesopore channels in the outer shells are radially aligned (Figure 2d). This unique pore orientation makes the hollow space highly accessible for guest molecules. It is noteworthy that, the hollow space size of the yolk-shell microspheres can be readily increased from 320 to 370 and 430 nm by simply increasing the thickness of the RF shell from 25, 50 and 80 nm, respectively (Figure S2); meanwhile, the pore size and the shell thickness of mesoporous silica can remain as 2.2 nm and 50 nm. Accordingly, the three samples were denoted as YS-320, YS-370, YS-430, respectively. The well-designed structure has silica-protected magnetite core, and easily tunable hollow space and highly accessible perpendicular mesoporous shells, making them different from other yolk-shell materials.

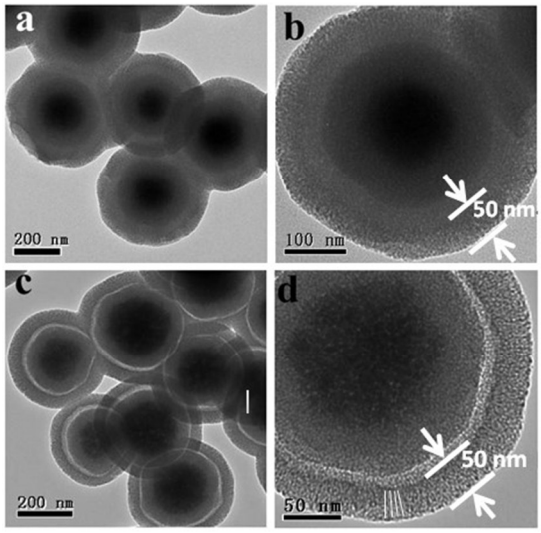

Figure 2. TEM images of the multi-shelled Fe_3O_4@SiO_2@RF@CTAB/SiO_2 microspheres with an outer shell of ~ 50 nm thick CTAB/silica composite (a, b) and the yolk-shell Fe_3O_4@SiO_2@hollow mSiO_2 microspheres (c, d) with different magnifications obtained after calcination treatment.

N_2 adsorption-desorption isotherms of YS-320 show representative type-IV curves with a sharp capillary condensation step, indicating cylindrical pores with a narrow pore size (Figure 3a). The pore size distribution curve derived from the adsorption branch indicates that the YS-320 sample has a mean pore size of ~ 2.2 nm (Figure 3a, inset). The BET surface area and total pore volume were calculated to be ~ 405 m^2/g and 0.3 cm^3/g, respectively. Wide-angle XRD patterns of YS-320 display the characteristic diffraction peaks assigned to magnetite phase and the amorphous silica (Figure s3). This result clearly indicates that the magnetic component in the composite is well retained in the whole synthesis process. Magnetic property characterization (Figure 3b) using a magnetometer at 300 K reveals that Fe_3O_4 particles, $Fe_3O_4@SiO_2$, and YS-320 have magnetization saturation values of 74.8, 62.5, and 23.5 emu/g, respectively. Additionally, no remanence was detected for all of the samples, reflecting a super-paramagnetic property. The samples YS-370 and YS-430 synthesized following the same synthesis procedure as that for YS-320 show similar magnetic properties and pore parameters (Table 1).

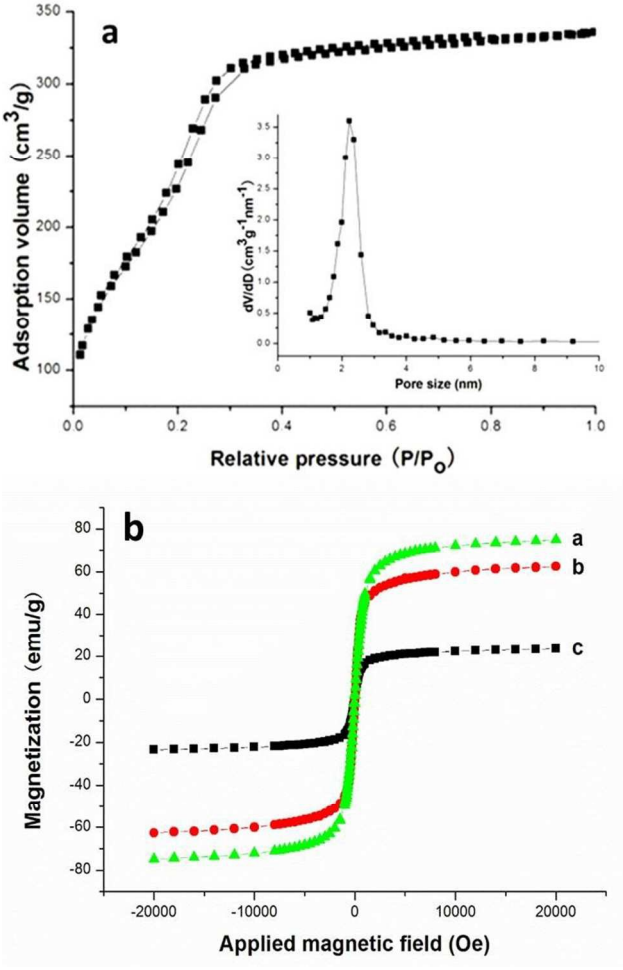

Figure 3. (a) Nitrogen adsorption-desorption isotherms and the corresponding pore size distributions (inset) of $Fe_3O_4@SiO_2@$hollow $mSiO_2$ microspheres (YS-320), and (b) The magnetic hysteresis loops recorded at 25 °C. (a) Fe_3O_4 particles, (b) $Fe_3O_4@SiO_2$ microspheres, and (c) $Fe_3O_4@SiO_2@$hollow $mSiO_2$ microspheres (YS-320).

Table 1. Textural properties and magnetic property of the samples.

Sample	BET surface area (m^2/g) [a]	Pore volume (cm^3/g) [b]	Pore size (nm) [c]	Magnetization value (emu/g)
YS-320	405	0.30	2.2	23.5
YS-320-Au	380	0.29	2.2	22.1
YS -370	418	0.35	2.2	21.0
YS-370-Au	393	0.31	2.2	19.0
YS -430	435	0.38	2.2	19.3
YS-430-Au	398	0.31	2.2	18.4

[a] The BET specific surface areas evaluated in p/p_0 from 0.05 to 0.35. [b] The total pore volumes estimated based on the volume adsorbed at P/P_0 ~ 0.992. [c] The pore sizes derived from the adsorption branches of the isotherms by using the BJH method.

The unique structure of the well-designed yolk-shell magnetic mesoporous silica microspheres (*i. e.* large hollow space, high magnetization, perpendicularly aligned mesopore channels) makes them an ideal candidate for various applications. It is well known that, Au nanoparticles exhibit good catalytic performances; however, they are apt to be washed away from the supports during reaction and/or recycling. Our designed yolk-shell magnetic mesoporous silica microspheres hold a great promise to overcome these problems. Here, in this study, sub-5 nm gold nanoparticles were loaded into the void space and immobilized on the $Fe_3O_4@SiO_2$ core via an in-situ reduction method.[56] Taking YS-320 as an example, after loading Au nanoparticles, the obtained YS-320-Au sample with embedded Au nanoparticles retains the yolk-shell structure, as evidenced by the TEM image (Figure 4a). The magnified TEM image (Figure 4b) reveals that Au nanoparticles are uniformly located in the hollow space. Scanning transmission electron microscopy high-angular annular dark-field (HAADF-STEM) image (Figure 5a) of single yolk-shell microsphere with supported Au nanoparticles clearly confirms that the yolk-shell structure and the Au nanoparticles are mainly located in the hollow space, and only some of them are trapped in the porous shell. The corresponding energy dispersive X-ray (EDX) mapping of Au element also shows that the gold nanoparticles are distributed in the matrix surrounded by Si and O (Figure 5b-d), confirming the confinement of Au nanoparticles in the yolk-shell mesoporous silica. High-resolution TEM image (Figure 4d) clearly indicates the crystal lattice of single gold nanoparticle. Selected area electron diffraction (SAED) patterns recorded on a YS-320-Au microsphere shows spotty diffraction rings which can be exactly assigned to Au nanoparticles with face centered cubic (*fcc*) structure (Figure 4d, inset). Wide-angle XRD patterns display both typical characteristic broad

diffraction peaks indexed to Au nanoparticles and Fe_3O_4 particles (Figure s3). According to the Debye-Scherrer formula, the mean crystalline size of gold nanoparticles was calculated about 4.2 nm. N_2 adsorption-desorption measurement indicates the composite catalyst has surface area of ~ 380 m^2/g and pore volume of 0.29 cm^3/g. Because Au nanoparticles' diameter is larger than that of the mesopore (~ 2.2 nm), the Au nanoparticles can be stably trapped in the yolk-shell microspheres, which helps to prevent the loss of precious gold nanoparticles in practical applications, especially for catalysis in liquid phases.

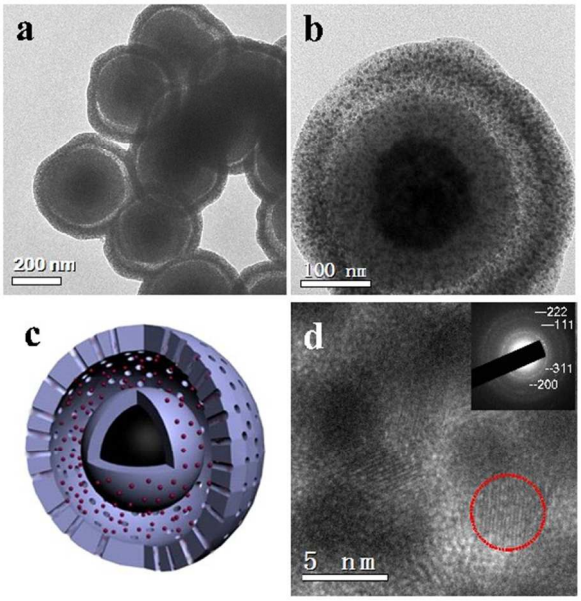

Figure 4. TEM images (a, b) and the structure model (c) of the yolk-shell magnetic mesoporous silica structures (YS-320-Au) with embedded gold nanoparticles (d) The corresponding HRTEM image of the gold nanoparticles and the inset is the SAED pattern of the gold nanoparticles.

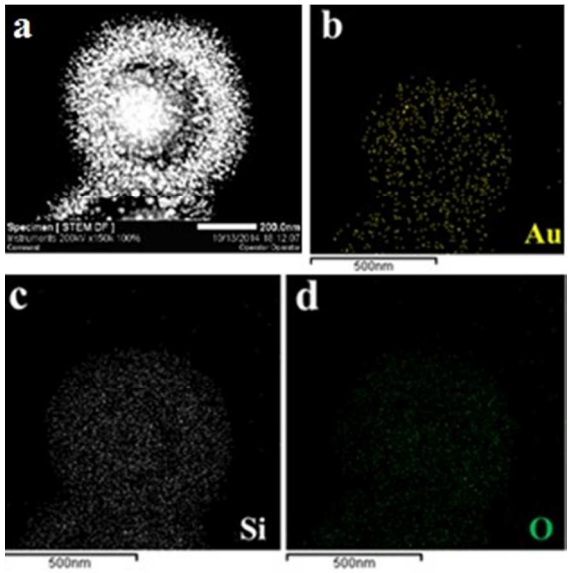

Figure 5. HAADF-STEM image (a) and energy-dispersive X-ray element mapping of Au (b), Si (c) and O (d) elements in a single yolk-shell microsphere with supported Au nanoparticles (YS-320-Au).

Styrene epoxidation is very important for producing styrene oxide which is an indispensable organic intermediate in chemical and biomedical industries. Styrene oxide is conventionally produced through the epoxidation of styrene using peracids. As is well known, peracids are extremely corrosive and unsafe to handle, and their use will make the purification process for products very difficult and create lot of waste. Au nanoparticles have been intensively studied as an excellent heterogeneous catalyst for styrene epoxidation. Herein, in this study, in order to investigate the catalytic performance of the synthesized Fe_3O_4@SiO_2@hollow mSiO_2-Au microspheres, styrene epoxidation reactions were carried out at 82 °C under argon atmosphere using *tert*-butylhydroperoxide (TBHP) as an oxidant and YS-320-Au, YS-370-Au, YS-430-Au as the heterogeneous catalysts, respectively. The products consist of benzaldehyde, styrene oxide and traces of benzoic acid according to GC-MS measurement. From Figure 6a, it can be seen that as the reaction proceeds, the conversion of styrene gradually increases to 99.3 %, 93.3 %, and 83.9 % for the samples YS-430-Au, YS-370-Au, YS-320-Au, respectively. It implies that larger hollow space favors the reactions due to the fast diffusion of reactants and product molecules. The three catalysts show different selectivity toward styrene oxide (Figure 6b). In the early stage of reaction, the selectivity of the sample YS-320-Au increases quickly to 86.5 % at 2 h; however, it drops dramatically as the reaction proceeds and reach 84.8 % at 4 h, and 72.9 % at 8 h, respectively. By contrast, the selectivity towards styrene oxide of the catalysts with larger hollow space increases to a peak value of 83.0 % for YS-370-Au at 4 h and 88.0 % for the YS-430-Au at 8 h, indicating that larger hollow space favors better selectivity for a longer reaction time. Therefore, it seems that the catalyst with smaller hollow space only accommodate relatively smaller amounts of styrene, thus leading to lower conversion; on the other hand, the product molecules after oxidation cannot diffuse away quickly from the supported Au nanoparticles in a short time, resulting in a lower selectivity probably due to the over-oxidation. From a comprehensive evaluation in terms of conversion and selectivity, the yolk-shell YS-430-Au sample displays a high conversion (91.4 %) and selectivity (82.8 %) after reaction for 12 h, which is much higher than that of previous reports based magnetic core-shell mesoporous silica,[23] or other porous materials as the supports.[60-63] The improved catalytic performance of the yolk-shell YS-430-Au sample is mainly due to its larger hollow space that helps reactants to contact with highly confined Au nanoparticles and facilitates the diffusion of product molecules for avoiding oxidation. Moreover, by utilization of the magnetic separability, the yolk-shell catalysts (*e. g.* YS-430-Au) can be easily separated and recycled with a magnet (2000 Oe), and the recycled YS-430-Au still exhibits outstanding structural stability (Figure S4) and excellent catalytic performance without significant decrease in both conversion (89.6%) and selectivity (81.5%) even after running 12 times (Figure 7). Wide-angle XRD patterns and electronic microscope measurements also confirm that the composition and mesoporous shell of the yolk-shell composite nanocatalysts are well-retained after running 12 times, indicative good structure stability. Inductively coupled plasma-atomic emission spectrometry (ICP-AES) measurements indicate that the Au content in the recycled catalysts is about 2.30 wt%, close to that

(2.32 wt %) of the as-made YS-430-Au sample. It suggests that Au nanoparticles are highly stable in the composite. Such an excellent catalytic performance and good recyclability is mainly attributed to the large hollow space, well-dispersed and stably confined Au nanoparticles, large surface area, and the unique perpendicular pore channels of the novel multifunctional nanocatalyst system.

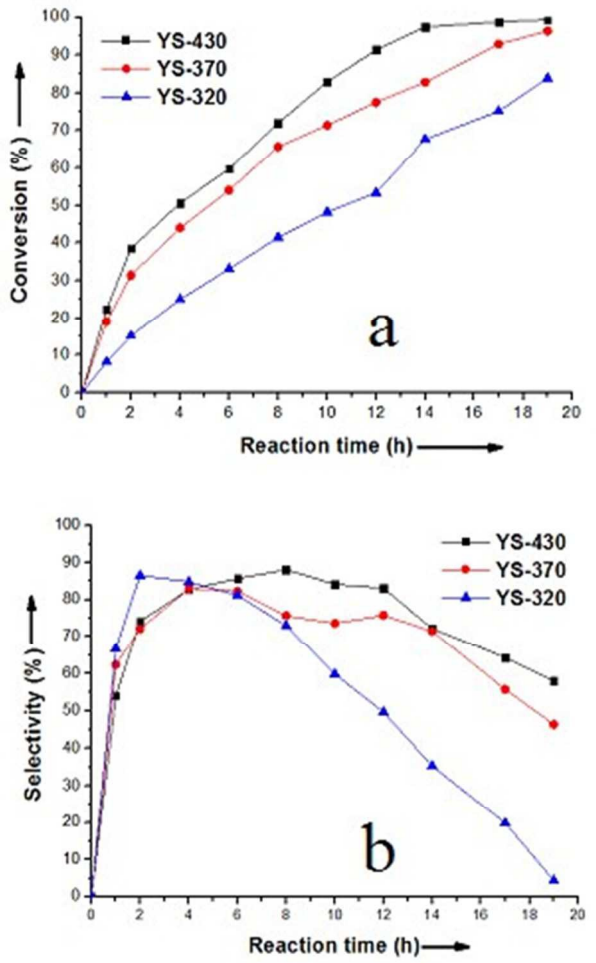

Figure 6. The catalytic performance of the yolk-shell microspheres supported Au nanoparticles (YS-320-Au, YS-370-Au, YS-430-Au) for the epoxidation of styrene at different reaction time, (a) the conversion of styrene, (b) the selectivity towards styrene oxide.

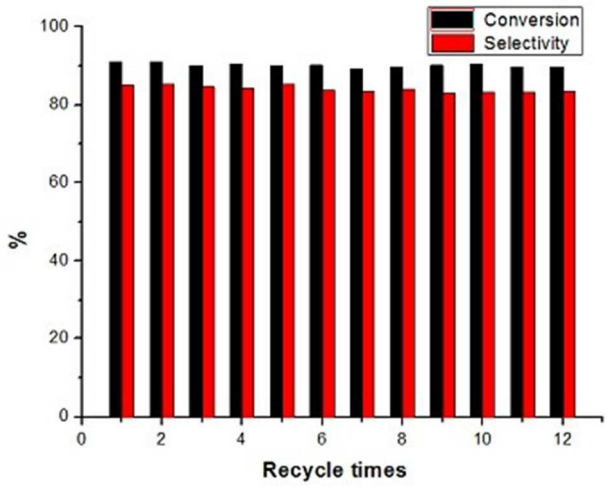

Figure 7 The catalytic performance of the recycled YS-430-Au catalyst for the epoxidation of styrene after using for 12 times.

Conclusions

In summary, we demonstrated a designed synthesis of a novel kind of yolk-shell magnetic mesoporous silica microspheres with well-configured structure through a combined interfacial sol-gel coating and surfactant-templating co-assembly method. The obtained yolk-shell Fe_3O_4@SiO_2@hollow mSiO_2 microspheres possess a well-defined nanostructure and highly integrated functions, large magnetization (up to 23.5 emu/g), open and ordered mesopore channels (2.2 nm), and controllable void space (320 - 430 nm). Through an in-situ reduction strategy, ultra-small gold nanoparticles (~ 4 nm) were deposited on the Fe_3O_4@SiO_2 yolk for the use as a highly confined but easily accessible nanocatalyst system. The multifunctional catalysts with large hollow space exhibit excellent catalytic performance for styrene epoxidation with high conversion of styrene (91.4 %) and selectivity (83.1 %) in 12 h due to the unique mesoporous hollow spherical structure. Through a simple magnetic separation, the yolk-shell nanocatalysts can be easily recycled with a magnetic field, and reused for catalysis without significant reduction of the catalytic performance even after use for 12 times. Additionally, the fabrication methodology of the novel catalysts opens up new possibilities in designing other yolk-shell structures with multiple components and highly integrated functionalities for various applications, such as drug delivery, sensing, disease diagnosis, and cancer hyperthermia.

Acknowledgements

This work was supported by the State Key 973 Program of PRC (2013CB934104), the NSF of China (51372041, 51422202), the specialized research fund for the doctoral program of higher education of China (20120071110007), the innovation program of Shanghai Municipal Education Commission (13ZZ004), Shanghai Rising Star Project of STCSM (12QH1400300), Program for New Century Excellent Talents in University (NCET-12-0123), and the "Shu Guang" Project (13SG02) supported by Shanghai Municipal Education Commission and Shanghai Education Development Foundation.

Notes and references

[a] Department of Chemistry, Advanced Materials Laboratory and State key Laboratory of Molecular Engineering of Polymers, Fudan University, Shanghai 200433, P. R. China

Electronic Supplementary Information (ESI) available: FT-IR spectra of (a) Fe_3O_4@SiO_2, (b) Fe_3O_4@SiO_2@RF, and (c) Fe_3O_4@SiO_2@hollow *m*SiO_2 (YS-320), TEM images of Fe_3O_4@SiO_2@hollow mSiO_2 microspheres YS-370 and YS-430 with different hollow space size of 370 and 160 nm and 430 nm, respectively. Wide-angle XRD patterns of Fe_3O_4 particles, YS-320 and YS-320-Au. TEM image of the recycled YS-430-Au catalysts after catalyzing the styrene epoxidation for 12 cycles. See DOI: 10.1039/b000000x/

1 C K. E. Sapsford, K. L. Tyner, B. J. Dair, J. R.Deschamps, and I. L. Medintz, *Anal. Chem.* 2011, **83**, 4453.
2 C. Liu, J. Tang, H. Chen, B. Liu and P.Yang, *Nano Lett*, 2013, **13**, 2989.
3 S. S. Kelkar, and T. M. Reineke, *Bioconjugate Chem.* 2011, **22**, 1879.
4 C. T. Kresge, M. E. Leonowicz, W. J. Roth, J. C. Vartuli and J. S. Beck, *Nature* 1992, **359**, 710.
5 D. Y. Zhao, J. L. Feng, Q. S. Huo, N. Melosh, G. H. Fredrickson, B. F. Chmelka and G. D. Stucky, *Science* **1998**, *279*, 548.
6 S. H. Joo, J. Y. Park, C. K. Tsung, Y. Yamada, P. D. Yang and G. A. Somorjai, *Nat. Mater.* 2009, **8**, 126.
7 A. H. Lu, J. J. Nitz, M. Comotti, C. Weidenthaler, K. Schlichte, C. W. Lehmann, O. Terasaki and F. Schuth, *J. Am. Chem. Soc.* 2010, **132**, 14152.
8 F. de Clippel, M. Dusselier, R. Van Rompaey, P. Vanelderen, J. Dijkmans, E. Makshina, L. Giebeler, S. Oswald, G. V. Baron, J. F. M. Denayer, P. P. Pescarmona, P. A. Jacobs and B. F. Sels, *J. Am. Chem. Soc.* 2012, **134**, 10089.
9 M. Stratakis and H. Garcia, *Chem. Rev.* 2012, **112**, 4469.
10 M. S. Chen and D. W. Goodman, *Science* 2004, **306**, 252.
11 S. Panigrahi, S. Basu, S. Praharaj, S. Pande, S. Jana, A. Pal, S. K.Ghosh and T. Pal, *J. Phys. Chem.* C 2007, **111**, 4596.
12 D. I. Enache, J. K. Edwards, P. Landon, B. Solsona-Espriu, A. F. Carley, A. A. Herzing, M. Watanabe, C. J. Kiely, D. W. Knight, and G. J. Hutchings, *Science* 2006, **311**, 362
13 M. D. Hughes, Y. J. Xu, P. Jenkins, P. McMorn, P. Landon, D. I. Enache, A. F. Carley, G. A. Attard, G. J. Hutchings, F. King, E. H. Stitt, P. Johnston, K. Griffin, and C. J. Kiely, *Nature* 2005, **437**, 1132.
14 A. Stephen, K. Hashmi, and G. J. Hutchings, *Angew. Chem. Int. Ed.* 2006, **45***,* 7896.
15 R. Sardar, A. M. Funston, P. Mulvaney, and R. W. Murray, *Langmuir* 2009, **25**, 13840.
16 M. Haruta, T. Kobayashi, H. Sano, and N. Yamada, *Chem. Lett.* 1987, **16**, 405.
17 M. Haruta, *Catal. Today* 1997, **36**, 153.
18 A. Saji, T. Ashutosh, *J. Nanosci. Nanotechno.* 2015, **3**, 1869.
19 M. Tominaga, T. Shimazoe, M. Nagashima, H. Kusuda, A. Kubo, Y. Kuwahara, and I. *J.* Taniguchi, *Electroanalytical Chemi.* 2006, **590**, 37.
20 A. Corma, and H. Garcia, *Chem. Soc. Rev.* 2008, **37**, 2096.
21 M. T. Bore, H. N. Pham, E. E. Switzer, T. L. Ward, A. Fukuoka, and A. K. Datye, *J. Phys. Chem.* B 2005, **109**, 2873.
22 T. Wang, J. N. Shangguang, W. Jiang, and Q. *J.* Zhong, *Solid State Chem.* 2014, **215**, 67
23 Y. H. Deng, Y. Cai, Z. K. Sun, J. Liu, C. Liu, J. Wei, W. Li, C. Liu, Y. Wang, and D. Y. Zhao, *J. Am. Chem. Soc.* 2010, **132**, 8466;
24 J. Pak, and H. Yoo, *Micropor. Mesopor. Mater.* 2014, **185**, 107.
25 T. T. Zhang, H. Y. Zhao, S. N. He, K. Liu, H. Y. Liu, Y. D. Yin, C. B. Gao, *ACS Nano* 2014, **8**, 7297.
26 C. H. Kuo, Y. Tang, L. Y. Chou, B. T. Sneed, C. N. Brodsky, Z. P. Zhao, and C.-K. Tsung, *J. Am. Chem. Soc.* 2012, **134**, 14345.
27 J. Liu, S. Z. Qiao, S. B. Hartono, and G. Q. Lu, *Angew. Chem. Int. Ed.* 2010, **49**, 4981.
28 J. Liu, H. Q. Yang, F. Kleitz, Z. G. Chen, T. Y. Yang, E. Strounina, G. Q. Lu, and S. Z. Qiao, *Adv. Funct. Mater.* 2012, **22**, 591.
29 H. Pan, J. Zhuang, L.-Y. Chou, H. K. Lee, X. Y. Ling, Y.-C. Chuang, and C.-K. Tsung, *J. Am. Chem. Soc.* 2014, **136**, 10561.
30 J. Liu, S. Z. Qiao, J. S. Chen, X. W. Lou, X. R. Xing, and G. Q. Lu, *Chem. Commun.* 2011, **47**, 12578.
31 J. S. Chen, D. Y. Luan, C. M. Li, C. F. Y. Boey, S. Z. Qiao, and X. W. Lou, *Chem. Commun.* 2010, **46**, 8252.
32 L. F. Tan, C. Dong, H. Y. Liu, and F. Q. Tang, *Adv. Mater.* 2010, **22**, 4885.
33 J. Lee, J. C. Park, H. Song, and *Adv. Mater.* 2008, **20**, 1523.
34 M. Sindoro, S. Granick, *J. Am. Chem. Soc.* 2014, **136**, 13471.
35 Y. Chen, H. R. Chen, M. Ma, F. Chen, L. M. Guo, L. X. Zhang, and J. L. Shi, *J. Mater. Chem.* 2011, **21**, 5290.
36 L. Zhang, S. Z. Qiao, Y.G. Jin, Z. G. Chen, H. C. Gu, and G. Q. Lu, *Adv. Mater.* 2008, **20**, 805.
37 H. X. Wu, G. Liu, S. J. Zhang, J. L. Shi, L. X. Zhang, Y. Chen, F. Chen, and H. R. Chen, *J. Mater. Chem.* 2011, **21**, 3037.
38 J. Kim, J. E. Lee, J. Lee, J. H. Yu, B. C. Kim, K. An, Y. Hwang, C. H. Shin, J. G. Park, J. Kim, and T. Hyeon, *J. Am. Chem. Soc.* 2006, **128**, 688.
39 W. R. Zhao, H. R. Chen, Y. S. Li, L. Li, M. D. Lang, and J. L. Shi, *Adv. Funct. Mater.* 2008, **18**, 2780.
40 C. Galeano, C. Baldizzone, H. Bongard, *Adv. Funct. Mater.* 2014, **24**, 220-232.
41 S. Ikeda, S. Ishino, T. Harada, N. Okamoto, T. Sakata, H. Mori, S. Kuwabata, T. Torimoto, and M. Matsumura, *Angew. Chem.Int. Ed.* 2006, **118**, 7221.
42 P. M. Arnal, M. Comotti, and F. Schüth, *Angew. Chem.Int. Ed.*2006, **118**, 8404.
43 I. Lee, J. B. Joo, Y. D. Yin, and F. Zaera, *Angew. Chem. Int. Ed.*2011, **50**, 10208.
44 J. C. Park, H. Song, *Nano Res.* 2011, **4**, 33.
45 X. L. Fang, Z. H. Liu, M. F. Hsieh, M. Chen, P. X. Liu, C. Chen, and N. F. Zheng, *ACS Nano,*2012, **6**, 4434.
46 X. B. Li, Y. Yang, and Q. H. Yang, *J. Mater. Chem.* A, 2013, **1**, 1525.
47 C. H. Kuo, Y. Tang, L. Y. Chou, B. T. Sneed, C. N. Brodsky, Z. P. Zhao, and C. K. Tsung, *J. Am. Chem. Soc.*2012, **134**, 14345.
48 J. H. Gao, G. L. Liang, B. Zhang, Y. Kuang, and X. X. Zhang, *J. Am. Chem. Soc.* 2007, **129**, 1428.
49 J. H. Gao, G. L. Liang, J. S. Cheung, Y. Pan, Y. Kuang, F. Zhao, B. Zhang, X. X. Zhang, E. X. Wu, and B. Xu, *J. Am. Chem. Soc.* 2008, **130**, 11828.
50 J. Liu, S. Z. Qiao, J. S. Chen, X. W. Lou, X. R. Xing, and G. Q. (Max)Lu, *Chem. Commun.* 2011, **47**, 12578.
51 W. M. Zhang, J. S. Hu, Y. G. Guo, S. F. Zheng, L. S. Zhong, W. G. Song, and L. J. Wan, *Adv. Mater.* 2008, **20**, 1160.
52 J. Liu, H. Xia, D. F. Xue, and L. Lu, *J. Am. Chem. Soc.* 2009, **131**, 12086.
53 Y. J. Hong, M. Y. Son, and Y. C. Kang, *Adv. Mater.* 2013, **25**, 2279.
54 J. M. Won, S. H. Choi, Y. J. Hong, *Sci. Rep.* 2014, **4**, 5857.

55 J. Liu, Z. K. Sun, Y. H. Deng, Y. Zou, C. Y. Li, X. H. Guo, L. Q. Xiong, Y. Gao, F. Y. Li, and D. Y. Zhao, *Angew. Chem. Int. Ed.* 2009, **48**, 5875.

56 H. G. Zhu, C. D. Liang, W. F. Yan, S. H. Overbury, and S. *J.* Dai, *Phys. Chem.* B. 2006, **110**, 10842.

57 A. B. Fuertes, V. V. Patricia, M. Sevilla, *Chem. Commun.* 2012, **48**, 6124.

58 S. Gu, T. Mogi, M. Konno, *J. Colloid Interface Sci.* 1998, **207**, 249.

59 W. Stöber, A. Fink, *J. Colloid Interface Sci.* 1967, **26**, 62.

60 J. Wei, Q. Yue, Z. K. Sun, Y. H. Deng, and D. Y .Zhao, *.Angew. Chem.Int. Ed*. 2012, **51**, 6149.

61 Y. H. Li, J. Wei, W. Luo, C. Wang, W. Li, S. S. Feng, Q. Yue, M. H. Wang, A. A. Elzatahry, Y. H. Deng, and D. Y. Zhao, *Chem. Mater.* 2014, **26**,2438.

62 V. R. Choudhary, D. K. Dumbre, N. S. Patil,; B. S. Uphade, and S. K. *J.* Bhargava, *Catal. Commun.* 2013, **300**, 217.

63 N. Linares, C. P. Canlas, J. Garcia-Martinez, and T .J. Pinnavaia, *Catal. Commun*. 2014, **44**, 50.

Graphic Abstract for TOC

Multifunctional yolk-shell microspheres comprising magnetite@silica supported Au nanoparticles and mesoporous silica with well-configured nanostructure were rationally synthesized through a combined interfacial sol-gel coating and surfactant-templating co-assembly method. The obtained microspheres are demonstrated as efficient and easily recyclable nanocatalysts for catalytic epoxidation of styrene with high conversion and good selectivity.